The ageing response of direct laser deposited metastable β-Ti alloy, Ti–5Al–5Mo–5V–3Cr

Sharma, D, Kada, SR, Fabijanic, D, Parfitt, D, Chen, B, Roebuck, B, Fitzpatrick, ME & Barnett, MR

Original citation & hyperlink:
Sharma, D, Kada, SR, Fabijanic, D, Parfitt, D, Chen, B, Roebuck, B, Fitzpatrick, ME & Barnett, MR 2021, 'The ageing response of direct laser deposited metastable β-Ti alloy, Ti–5Al–5Mo–5V–3Cr', Additive Manufacturing, vol. 48, no. Part A, 102384.
https://dx.doi.org/10.1016/j.addma.2021.102384

DOI 10.1016/j.addma.2021.102384
ISSN 2214-7810
ESSN 2214-8604

Publisher: Elsevier

The ageing response of direct laser deposited metastable β-Ti alloy, Ti–5Al–5Mo–5V–3Cr

Deepak Sharma[a,b,*], Sitarama Raju Kada[b], Daniel Fabijanic[b], David Parfitt[a], Bo Chen[a,c], Bryan Roebuck[d], Michael E. Fitzpatrick[a], Matthew Robert Barnett[b]

[a] The Institute for Future Transport and Cities, Coventry University, Coventry, CV1 5FB, UK

[b] The Institute for Frontier Materials, Deakin University, Victoria, 3216, Australia

[c] Department of Engineering, University of Leicester, Leicester, LE1 7RH, UK

[d] National Physical Laboratory, Teddington, London, TW11 0LW, UK

*Corresponding author's e-mail addresses - sharmad9@uni.coventry.ac.uk; sdeepa@deakin.edu.au

Abstract

The formation of solely β-phase titanium after direct laser deposition (DLD) of metastable β-Ti alloy does not provide the desired properties. Hence, we present a study into the ageing response of DLD built Ti-5553 β-Ti alloy to obtain the bimodal (β+α) microstructure providing improved properties. The results obtained from the heat treatments showed that a unique microstructure with refined intragranular and discontinuous grain boundary α-phase can be obtained by directly ageing (using fast heating rate) the as-built samples at the ageing condition (600 °C + 0.5 h). This microstructure produced a good balance in mechanical properties (UTS = 1345 ± 5 MPa and δ = 11.6 ± 0.5 %). The interparticle spacing between the α-phase (d) showed a correlation with microhardness ($H_v = 340 + 158/\sqrt{d}$) and yield stress ($\sigma_{0.2} = 870 + 15086/\sqrt{d}$) values for all the aged samples.

Keywords

Titanium alloys; Direct laser deposition; Single and duplex aging; Microstructure-property relationship

1. Introduction

Ti–5Al–5Mo–5V–3Cr wt% (Ti-5553) is a metastable β-Ti alloy that offers a high ultimate tensile strength of ~1265 MPa and a decent ductility of ~10% in the cast and forged conditions, *i.e.* wrought material [1]. These properties of the alloy are dependent on the final microstructure, which itself is sensitive to the heat treatment conditions such as cooling rate, heating rate, ageing temperature and ageing time [2–4].

Typically after single ageing of homogenised material with the fast heating rate (~100 °C/min), the microstructure of the wrought alloy consists of allotriomorphic α-phase along the prior-β grain boundaries, and the Widmanstätten α-phase near the grain boundaries [5]; whilst, the intragranular α-phase exhibits acicular morphology with self-accommodated clusters of three α variants after single ageing [6]. Single ageing with the slow heating rate (~5 °C/min) and duplex ageing lead to extreme refinement of intragranular α-phase due to the metastable isothermal ω-phase (ω_{iso}) precipitate-assisted α-phase nucleation improving strength levels [7]. The formation of ω_{iso} precipitates happens below 450 °C either by low-temperature ageing or slowly heating (~5 °C/min) the sample to the desired temperature [3,8,9].

Additive manufacturing of titanium alloys for aerospace is attractive due to design and near-net-shape benefits [10]. There are several variants of additive manufacturing such as blown powder deposition, a form of direct laser deposition (DLD); and selective laser melting (SLM), a form of powder bed fusion [11]. DLD is beneficial because it provides a high deposition rate and a wider processing window to fabricate larger items in comparison to the other metal-based additive manufacturing methods [11].

Ti-5553 β-Ti alloy is mostly processed by SLM [12–14], where Carlton *et al.* [14] recently reported the influence of single ageing on the mechanical properties of SLM built Ti-5553 β-Ti alloy. However, the influence of different microstructural features, such as size, shape,

volume fraction, and distribution of α strengthening phase, on the mechanical properties was not studied. These characteristics of the α-phase are affected by different ageing conditions. Therefore, the study of microstructure evolution as a function of different ageing conditions such as single ageing with different heating rates and duplex ageing can help in optimising the mechanical properties.

The inherent rapid cooling rates associated with DLD led to the formation of solely β-phase in the as-built condition that does not provide the desired mechanical properties [12]. A bimodal (α+β) microstructure was produced after *in situ* dwelling (*i.e.* switching off the laser beam) and *in situ* annealing (*i.e.* laser scanning without feeding powder) after each layer to get the desired properties. However, an inhomogeneous microstructure was observed after *in situ* dwelling and *in situ* annealing that led to a variation in the microhardness at different locations [13]. The DLD samples showed anisotropy in the mechanical properties [15] and the aged samples showed better mechanical properties when compared to the most widely used mill annealed alloys [10]. Hence, post-processing of these samples was recommended to obtain the minimum required properties and performance consistency [10]. However, the ageing response of DLD built β-Ti alloys is not understood and requires the development of a specific post-processing pathway to obtain a substantial improvement in the properties of DLD built β-Ti alloys. The critical evaluation and understanding of DLD built β-Ti alloy will support the potential application of additive manufacturing (AM) in the aerospace sector. The microstructure of the AM samples just after deposition is unique and exhibits the presence of sub-structures in the β-phase grains [12]. Therefore, it is important to understand the influence of these sub-structures on the aged microstructures of additively manufactured Ti-5553 β-Ti alloy.

In this context, we present a study into the ageing response of AM Ti-5553 β-Ti alloy deposited using DLD. Different post-processing pathways, comprising single and duplex

ageing, for as-built samples were explored to critically understand the influence of heat treatment upon part microstructure and the mechanical properties. A range of ageing temperatures and ageing time were used to understand the microstructural evolution and its likely effect on mechanical properties. Some as-built samples were also solution-treated to remove the sub-structures formed and investigate the subsequent effect on microstructure after ageing. Tensile tests and microhardness measurements were performed to find out the influence of different aged microstructures on the mechanical properties of AM Ti-5553 β-Ti alloy.

2. Experimental details

2.1. Material deposition

Plasma-atomised spherical Ti-5553 β-Ti alloy powder was obtained from AP&C company as a starting material. The typical appearance of the as-received powder is shown in Fig. 1 (a). The particle size distribution of the powder was calculated using scanning electron microscopy (SEM) images, where the particle size (after measuring 150 particles) lied in the range of 16–148 μm; with an average value of 66 ± 34 μm. The backscattered electron (BSE) mode on a Zeiss Gemini Sigma 500VP SEM was used to perform all the SEM characterisations. An accelerating voltage of 20 kV was applied. The aperture size of 60 μm and a working distance of 6 mm was used. The chemical composition of the powder as measured using inductively coupled plasma atomic emission spectroscopy (ICP-AES) is presented in Table 1.

Double walls (40 mm × 10 mm × ~1.5 mm; 10 mm along the build direction) of Ti-5553 β-Ti alloy, as shown in Fig 1 (b), were manufactured in an OPTOMEC LENS MR-7 system equipped with a 1 kW IPG Fiber Laser System. The chemical composition of the as-built samples, measured using ICP-AES, is presented in Table 1. The Al content (4.98 wt%) of the as-built samples decreased with respect to the Al content (5.04 wt%) in the powder. This is because of the evaporation of Al at the high temperature of additive manufacturing processes

[16]. The oxygen content (0.1 wt%) in the as-built sample was found to be more than the oxygen content (0.065 wt%) in the powder. This is because of the oxygen pick up during high-temperature additive manufacturing processes [16]. The small samples were deposited for microstructural and microhardness characterisation. Bigger size double-wall samples (22 mm × 60 mm × 2 mm; 60 mm along the build direction) were deposited to extract the sub-size tensile test samples as per ASTM E8 standards. The laser power, feed rate and scanning speed during the build were 300 W, 6 g/min and 635 mm/min, respectively. The laser spot size was 0.25 mm. The oxygen concentration of the build chamber was maintained within the range of 2–18 ppm during the building process. The melt pool overlap was approximately 50% and the layer thickness along the build direction was 0.25 mm.

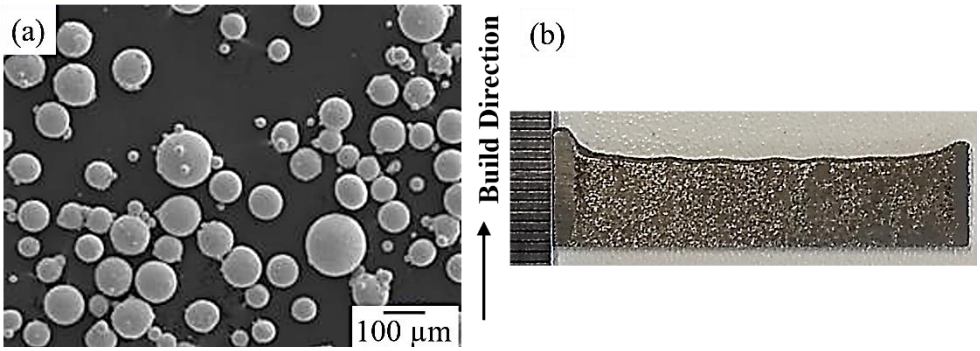

Fig. 1. (a) SEM micrograph of plasma-atomised spherical Ti-5553 β-Ti alloy powder used for depositing the alloy samples. (b) typical appearance of the double-wall sample after deposition.

Table 1. Chemical composition of the Ti-5553 β-Ti alloy powder and the as-built samples used in the current work.

Elements (wt%)	Mo	V	Al	Cr	Zr	Fe	Co	C	O	Nb	Ti
Powder	5.08	4.52	5.04	2.86	<0.01	0.36	<0.01	<0.01	0.065	<0.01	Bal
As-built Sample	5.10	4.54	4.98	2.86	<0.01	0.38	<0.01	0.01	0.1	<0.01	Bal

2.2. Heat treatments

The as-built samples were firstly ground using 320 grit size SiC abrasive paper to remove the oxide layer formed during deposition. The samples were then sectioned to create 10 mm × 10 mm × ~1.5 mm samples for heat treatments. A Bonderite L-GP Acheson coating was applied

to these ground samples to minimise the formation of α-case during the heat treatments. Subsequently, the coating was dried for a day before the heat treatments. The samples were either directly aged using single ageing or duplex ageing: duplex ageing comprised pre-ageing at 300 °C for 8 h and final ageing at a higher temperature. Two different heating rates (~100 °C/min and ~5 °C/min) were used during single ageing to understand the influence of heating rate on the evolved microstructure. Some of the as-built samples were first solution-treated at 900 °C for 0.5 h followed by water quenching before ageing. The solution treatment was done to remove the sub-structures formed during deposition and understand their subsequent effect on ageing.

For single ageing with higher heating rate, the samples were aged at 500 °C, 600°C and 700 °C for 0.5 h and 6 h. For single ageing with slower heating rate and duplex ageing, the samples were aged at 600°C for 0.5 h. The solution-treated samples were also aged at 600°C for 0.5 h using single ageing with faster heating rate. All the heat treatment experiments, carried out in the current work, are summarised in Table 2. These different ageing parameters were chosen to see their influence on the obtained microstructure and the associated mechanical properties. The heat treatment experiments were performed under an argon gas atmosphere with a flow rate of 10 l/min. All the aged samples were finally water-quenched to room temperature.

Table 2. Heat treatments applied to additively manufactured Ti-5553 β-Ti alloy. WQ refers to water quenching.

Approach	Material Initial Condition	Heat Treatment		
As-built plus single ageing with faster heating rate (~100 °C/min)	As-built	500 °C/0.5 h	WQ	
		500 °C/6 h	WQ	
		600 °C/0.5 h	WQ	
		600 °C/6 h	WQ	
		700 °C/0.5 h	WQ	
		700 °C/6 h	WQ	
As-built plus single ageing with slower heating rate (~5 °C/min)	As-built	600°C/0.5 h	WQ	
As-built plus duplex ageing	As-built	300 °C/8 h	600 °C/0.5 h	WQ
Solution-treated plus single ageing with faster heating rate (~100 °C/min)	Solution- treated (900 °C/0.5 h/WQ)	600 °C/0.5 h	WQ	

2.3. Material characterisation

The cross-section of the as-built, solution-treated, and aged samples was ground up to 1200 grit size SiC abrasive papers for characterisation. The samples were mounted in 2″ mount using the hot mounting procedure on a Struers' hot mounting machine (CitoPress-15) to examine the cross-section. Subsequently, the samples were polished up to 1 µm using diamond suspension followed by vibratory polishing using 0.02 µm particle size colloidal suspension. The samples were finally cleaned in an ultrasonic cleaner for 0.25 h using distilled water.

The samples were examined under X-ray diffraction (XRD) for phase analysis applying Cu-K_α X-ray radiation over a 2θ range of 35° to 100° at a slow scan rate of 1°/min. Previously published crystallographic data on Ti alloys [9,17,18] was used to identify the phases. Energy-dispersive spectroscopy (EDS) was performed to determine the elemental composition of the sub-structures observed in the as-built samples. The EDS was performed using X-Max^N detector from Oxford instruments installed in the same SEM machine. Electron backscatter diffraction (EBSD) was used to characterise the texture in the material. The NordlysNano detector from Oxford instruments was used for EBSD scans. An accelerating voltage of 20 kV

was used. The large area scans were collected using an aperture size of 300 μm and a step size of 0.2 μm. Channel 5 software was used to analyse the EBSD data. The microhardness values of the as-built, solution-treated, and aged samples were obtained using the Vickers micro-indentation (0.5 kgf load) method. An average of 40 measurements is reported for each sample.

ImageJ software was used to quantify the evolved microstructure of the as-built and the aged samples. For quantification of the microstructures using ImageJ, image processing was performed to obtain the drawings of the microstructures; by reducing the bandpass filter followed by the thresholding of the microstructure. The obtained drawings looked similar to the microstructures. One such example is shown in Supplementary Note 1.

Tensile tests were also conducted on the aged samples to find out the influence of different ageing approaches on the mechanical properties of the AM Ti-5553 β-Ti alloy. Samples aged at 600 °C for 0.5 h via different ageing approaches were selected for tensile tests, where the gauge length, the width of the gauge section and the thickness of the tensile test samples were kept as 12.7 mm, 3 mm, and 1 mm, respectively. The samples were extracted with the long axis along the build direction. The tensile tests were conducted at room temperature on a 10 kN Instron machine (servo-hydraulic) with a strain rate of 10^{-4}/s. Three samples were tested under each condition and the average data is presented here.

3. Results

3.1. Microstructural characterisation

3.1.1. As-built microstructure

The as-built samples showed the presence of spherical gas pores (19-62 μm) mostly distributed at the edges. The average number density per unit area was calculated as ~0.22 per mm^2. The EBSD map of the cross-section of the as-built sample is shown in Fig. 2 (a). The as-

built samples exhibited a homogeneous microstructure (Fig. 2 (b)), and XRD analysis (Fig. 3) confirmed the presence of solely β-phase in the as-built microstructure. This implies that the material may be aged directly rather than requiring a subsequent solution-treatment process as done with conventionally manufactured materials. The β grains become increasingly elongated towards the bottom of the as-built sample (Fig. 2 (a)), whilst more equiaxed grains were present at the top of the sample (Fig. 2 (a)). The width of the β grains (after measuring 100 grains) remained the same from bottom to top as 184 ± 66 µm. The as-built samples exhibited slight texture in the <100> direction, and the β grains grew along the build direction. The texture intensity was measured as 4 times random (Fig. 2 (c)). The scan (melt pool) tracks are also visible in the micrograph (Fig. 2 (b)) throughout the sample. The microstructure also consisted of sub-structures within the β grains. These sub-structures were of cellular morphology. If we look between two scan tracks (Fig. 2 (b)), the sub-structures are not present at the top of the n^{th} scan track; however, when approaching the $(n+1)^{th}$ scan track, the sub-structures are mainly present just below the $(n+1)^{th}$ scan track. The average sub-structure width was 14 ± 4 µm. The above observations remained true throughout the as-built sample, *i.e.* from bottom to top. Please see Supplementary Note 2.

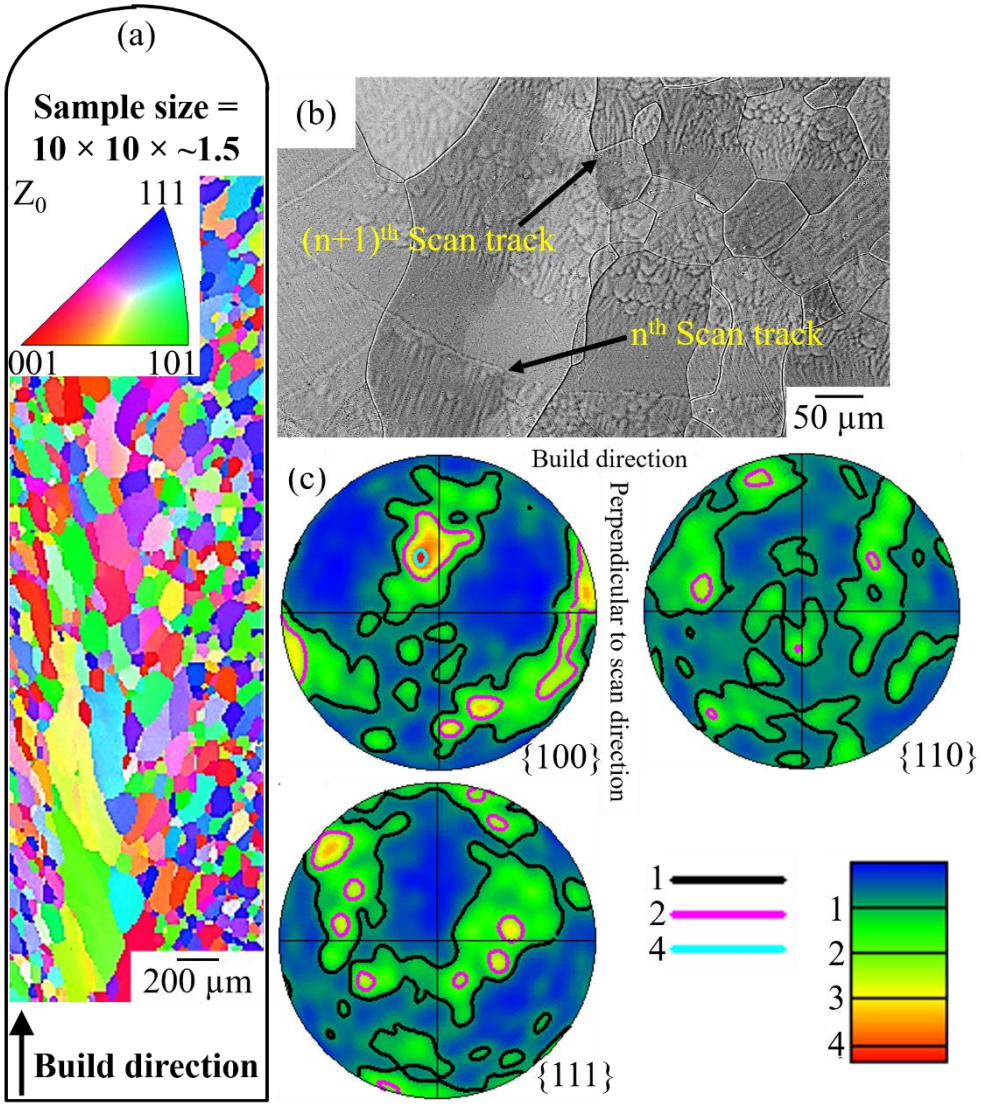

Fig. 2. (a) The EBSD map of the cross-section of the as-built sample showing the characteristics of β-phase along the build direction. (b) shows the SEM micrograph of the as-built sample showing the presence of solely β-phase and the cellular sub-structures after deposition. (c) shows the pole figures for the as-built sample taken along {100}, {110}, and {111}. The pole figures suggest that the β grains in the as-built samples have a preferential alignment along the <100> direction with texture intensity as 4 times random.

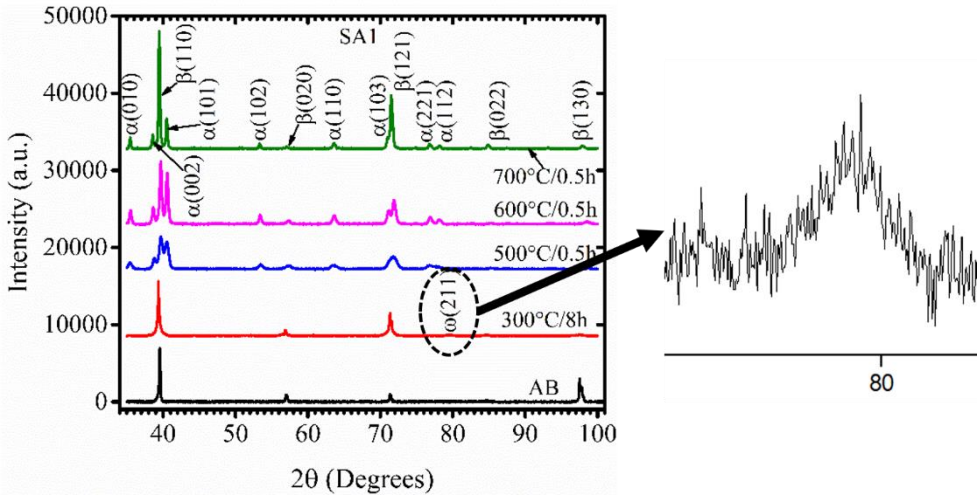

Fig. 3. The evolution of XRD diffraction patterns for as-built, pre-aged (300 °C + 8 h) and single-aged samples at different temperatures for 0.5 h after following single ageing with faster heating rate (SA1) approach. AB refers to the as-built sample. ω (211) peak observed after ageing for 8 h at 300 °C is also highlighted in the figure.

The elemental mapping (Fig. 4) of the as-built samples revealed that the sub-structure cores (Point 1) were slightly rich in Mo (6.3±0.2 wt%), whilst depleted in Cr (1.9±0.09 wt%). The sub-structure boundaries (Point 2) were slightly depleted in Mo (5.5±0.1 wt%) and rich in Cr (2.3±0.05 wt%). However, the remaining elements (Ti, V, and Al) were homogenous in the sub-structure. The results of the compositional analysis (after 40 measurements across the sample) done within the core of sub-structures, sub-structure boundaries and sub-structure free region of the as-built samples are shown in Table 3.

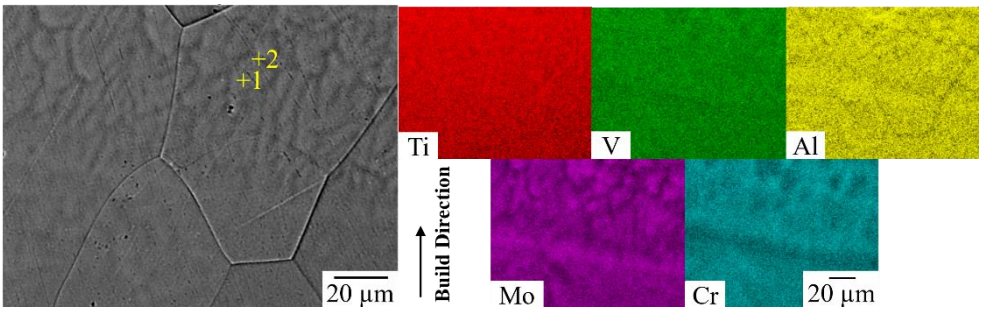

Fig. 4. The left-hand side image (grey colour) is an SEM image on which EDS mapping was performed. The EDS mapping results for the as-built samples are shown as the coloured maps. The maps indicate that the sub-structures (Point 1) are rich in Mo and depleted in Cr, whilst the sub-structure boundaries (Point 2) are rich in Cr but depleted in Mo.

Table 3. The compositional analysis (in wt%) of the sub-structure core, sub-structure boundaries and sub-structure free region in the as-built samples.

Region	Ti	V	Al	Mo	Cr
Sub-structure core	83.7±0.1	4.5±0.09	3.6±0.05	6.3±0.2	1.9±0.09
Sub-structure boundaries	83.9±0.1	4.6±0.1	3.7±0.05	5.5±0.1	2.3±0.05
Sub-structure free region	83.8±0.1	4.5±0.1	3.7±0.06	5.9±0.1	2.1±0.05

3.1.2. Heat-treated microstructure

The solution-treated sample did not show any presence of sub-structures, and only β-phase was present, as shown in Fig. 5 (a). The width of the β grains (after measuring 100 grains) was measured as 187 ± 66 μm, which is approximately the same as the as-built sample. No changes in the β grains were observed after solution treatment. Elongated β grains were still present in the microstructure. Please see Supplementary Note 3. This has also been seen previously for wrought alloy samples where solution treatment (at 900 °C for 0.5 h) did not cause any changes to β grains of Ti-5553 β-Ti alloy [1,9]. The as-built and the solution-treated samples showed differences in their subsequent ageing response. Fig. 5 (b) and (c) show the microstructures of the as-built and the solution-treated samples, respectively, following an ageing heat treatment (single ageing with faster heating rate) of 600 °C for 0.5 h. A generally more refined intragranular α-phase was observed for the as-built sample compared to the solution-treated sample after ageing. Both samples showed a similar self-accommodating acicular morphology of the intragranular α-phase. The solution-treated sample also showed Widmanstätten α-phase near grain boundaries in the aged condition, that grows from the grain boundary α-phase to the interior of the β grains. No Widmanstätten α-phase was observed near grain boundaries for aged as-built samples (Fig. 5 (b)). The volume fraction of the intragranular α-phase was similar (~52%) for both the aged samples. The width of the intragranular α-phase was larger for the solution-treated sample (139 ± 22 nm) compared to the as-built sample (105 ± 20 nm), based on a measurement of 150 α-phase. The interparticle (α-phase) spacing for as-built and solution-treated samples was found to be about 137 ± 17 nm and 187 ± 16 nm, respectively. The meaning

of width and interparticle spacing of intragranular α-phase is explained in Supplementary Note 4.

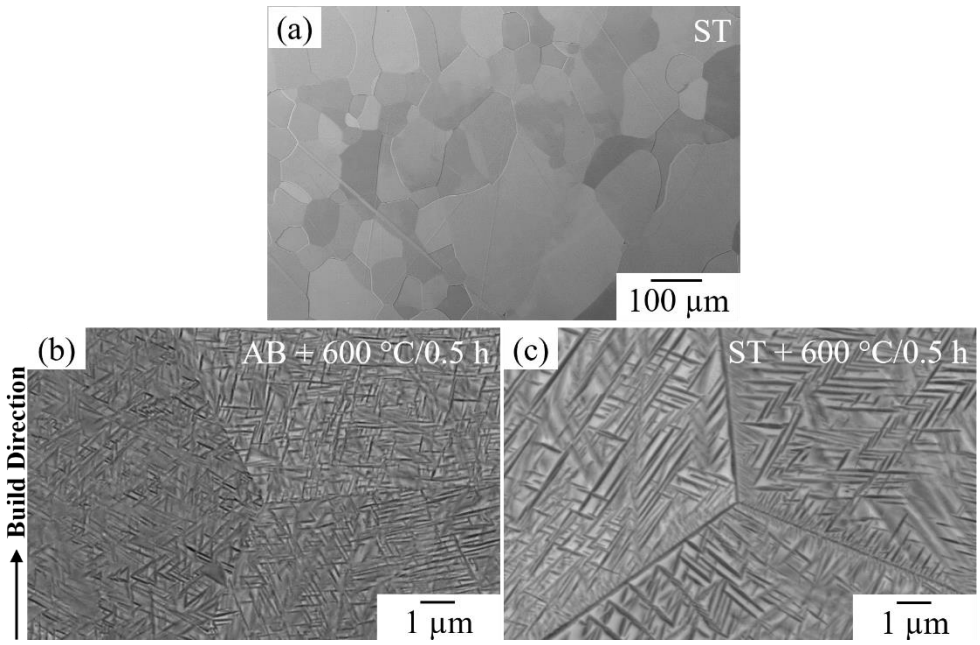

Fig. 5. (a) The BSE-SEM microstructure of the solution-treated (ST) sample showing the presence of solely β-phase without any sub-structures. (b) and (c) show the BSE-SEM microstructure of aged (600 °C/0.5 h) Ti-5553 β-Ti alloy directly after deposition (AB) and after solution treatment (ST), respectively, illustrating the grain boundary and intragranular α-phase characteristics.

It is also important to note here that the sub-structures were still visible (Fig. 6 (a)) in the aged microstructure. The elemental mapping results for the aged samples are shown in Fig. 7. The results of the composition analysis (after 40 measurements across the sample) done within the core of sub-structures, sub-structure boundaries and sub-structure free region of the aged samples are shown in Table 4. Similar to the as-built samples, the aged samples exhibited Mo rich (6.1±0.1 wt%) and Cr depleted (1.9±0.1 wt%) sub-structure cores, and Cr rich (2.5±0.05 wt%) and Mo depleted (5.3±0.1 wt%) sub-structure boundaries.

The width and morphology of the α-phase precipitates remained uniform within sub-structure and sub-structure free regions, *i.e.*, there was no observable difference in the microstructure of the aged samples when examined within the sub-structures and sub-structure-free regions, as shown in Fig. 6. In addition, thinner and discontinuous grain boundary α-phase

was observed for the as-built sample (Fig. 5 (b)), whilst a thicker and continuous grain boundary α-phase was observed for the solution-treated (Fig. 5 (b)) sample after ageing. The as-built and the solution-treated samples, after ageing, did not show any observable difference in the width and morphology of the α-phase along the build height.

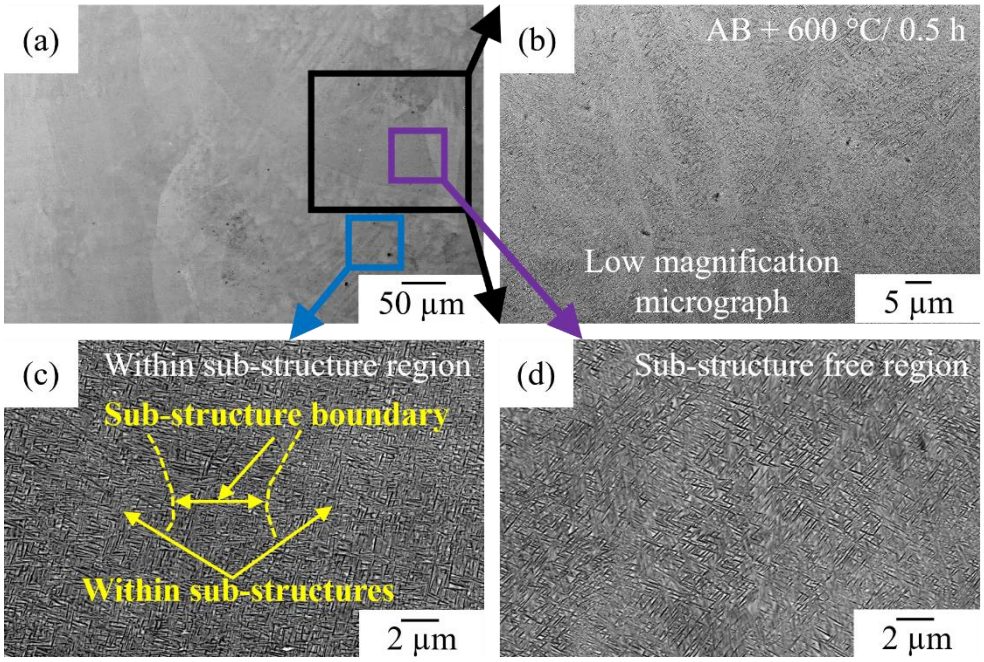

Fig. 6. BSE-SEM microstructure of aged (600 °C/0.5 h) Ti-5553 β-Ti alloy showing (a) the presence of sub-structures after ageing. (b) shows low magnification SEM micrograph showing the uniform distribution of intragranular α-phase across the sub-structures and sub-structure free regions. AB refers to the as-built sample. (c) and (d) show the high magnification SEM micrographs from sub-structures and sub-structure free regions, respectively. No observable difference in the α-phase characteristics was observed across the different regions.

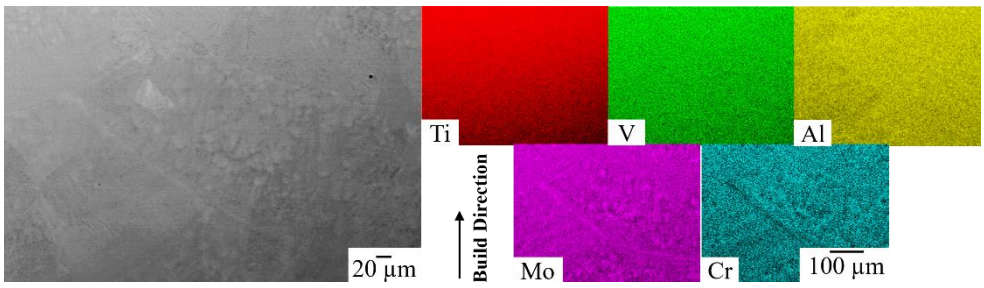

Fig. 7. The left-hand side image (grey colour) is an SEM image on which EDS mapping was performed. The EDS mapping results for the aged samples (600 °C/0.5 h; using fast heating rate) are shown as the coloured maps. The maps indicate that the sub-structures are rich in Mo and depleted in Cr, whilst the sub-structure boundaries are rich in Cr but depleted in Mo.

Table 4. The compositional analysis (in wt%) of the sub-structure core, sub-structure boundaries and sub-structure free region in the aged samples.

Region	Ti	V	Al	Mo	Cr
Sub-structure core	83.8±0.2	4.6±0.09	3.8±0.05	6.1±0.1	1.9±0.1
Sub-structure boundaries	83.9±0.2	4.7±0.05	3.7±0.08	5.3±0.1	2.5±0.05
Sub-structure free region	83.9±0.1	4.5±0.1	3.8±0.06	5.6±0.1	2.2±0.05

The BSE-SEM microstructures of the samples aged by single ageing with slow heating rate and duplex ageing approaches but with a common treatment step (600 °C + 0.5 h), are shown in Fig. 8 (a) and (b), respectively. The microstructures showed the presence of extremely refined α-phase precipitates uniformly distributed within the β-phase grains. The duplex-aged and slow-heated single-aged samples exhibited similar microstructures. However, a more refined microstructure was obtained in these cases when compared to the fast-heated single-aged samples (as-built and solution-treated).

The presence of α-phase in the as-built plus single-aged microstructures after ageing at different temperatures (500 °C, 600 °C, and 700 °C) with fast heating rate can also be confirmed from the XRD analysis (Fig. 3). The sample aged at 300 °C for 8 h during duplex ageing showed the presence of a small volume fraction of isothermal ω-phase in the XRD data (Fig. 3); however, no α-phase was observed after ageing at 300 °C for 8 h.

A relatively thicker and continuous grain boundary α-phase was observed after single ageing with slower heating rate, and after duplex ageing when compared to the as-built samples directly aged using single ageing with faster heating rate. Very thin precipitate-free-zones (PFZ) were also observed near the grain boundaries for the slow-heated single-aged and the duplex aged samples, whilst the fast-heated single-aged as-built samples only showed PFZ after ageing at 700 °C (Supplementary Note 5). The morphology of the intragranular α-phase remained the same throughout the single ageing of the as-built samples with faster heating rate conditions. The samples aged at 700 °C showed thick and continuous grain boundary α-phase (Supplementary Note 5).

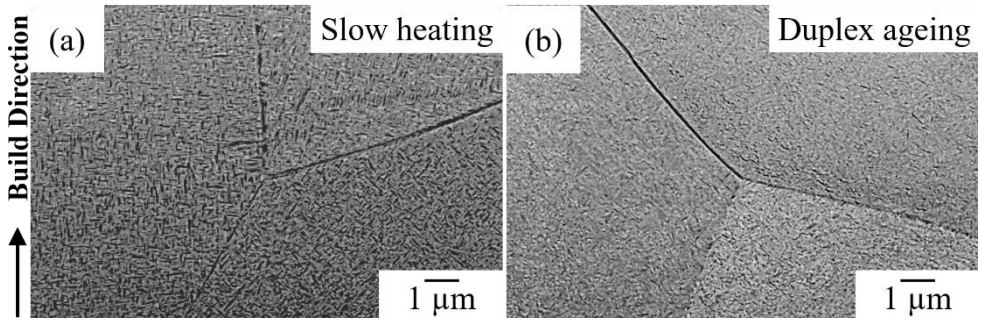

Fig. 8. The BSE-SEM microstructure of the additively manufactured Ti-5553 β-Ti alloy aged at 600 °C for 0.5 h using (a) single ageing with slower heating rate, and (b) duplex ageing.

Table 5 shows the quantified values of the aged microstructures in terms of volume fraction, width and interparticle spacing of the intragranular α-phase. An average of 150 measurements is reported for the width and interparticle spacing of the intragranular α-phase. The aged samples did not show any observable difference in the width and interparticle spacing of the α-phase along the build height.

For single ageing of the as-built samples with the faster heating rate, the maximum volume fraction of α-phase (~52%) was obtained for the samples aged at 600 °C, independent of ageing time (Table 5). The lowest volume fraction was observed at 700 °C. This is due to the proximity to the β-transus temperature (~850 °C). The volume fraction remained constant with increasing ageing time at 700 °C. At 500 °C, the volume fraction increased with an increase in the ageing time. Different ageing approaches showed similar (~52%) volume fraction of α-phase when the samples were aged at 600 °C for 0.5 h, *i.e.*, pre-ageing and heating rate have not affected the volume fraction of α-phase when aged at 600 °C for 0.5 h.

For single ageing of as-built samples with the faster heating rate, the width and interparticle spacing of α-phase increased with increased ageing temperature (Table 5). The width and interparticle spacing of α-phase remained constant as the ageing time was increased during ageing at 500 °C. However, the volume fraction increased. This indicates that the number density increases with ageing time leading to reduced interparticle spacing (Table 5). The reason for not coarsening with ageing time at this temperature is because the α-phase

precipitation initiates at near this temperature. The coarsest microstructures were obtained for the samples aged at 700 °C (Table 5). The observation of coarser intragranular α-phase at 700 °C is attributed to the availability of a larger diffusion rate at the higher temperature [19]. The width and interparticle spacing of α-phase for the samples aged at 700 °C remained approximately similar with increased ageing time. At 600 °C, the α-phase coarsened and interparticle spacing increased with ageing time. The precipitation of coarser α-phase leads to a region with more β-stabilisers in the surrounding region of the precipitates. The precipitation of α-phase is difficult in this region because of the high stability of the region due to enrichment in β-stabilisers. Hence, it gives a broader β stabilised region in the surrounding of the precipitates leading to higher interparticle spacing as stated above. The slow-heated single-aged and the duplex-aged samples showed extremely refined α-phase due to ω_{iso} assisted nucleation.

Table 5. The characteristic variation in volume fraction, width of intragranular α-phase, and interparticle spacing between the α-phase as a function of different ageing approaches.

Approach	Heat treatment condition		Volume fraction (%)	Width (nm)	Interparticle spacing (nm)
	Temperature (°C)	Time (h)			
As-built plus single ageing with faster heating rate	500	0.5	48.5	55 ± 15	110 ± 20
		6	50.6	60 ± 13	98 ± 18
	600	0.5	52.7	105 ± 20	137 ± 17
		6	52.8	118 ± 21	158 ± 16
	700	0.5	40.1	163 ±24	259 ± 38
		6	39.8	165 ± 22	266 ± 30
As-built plus single ageing with slower heating rate	600	0.5	52.8	81 ± 21	115 ± 15
As-built plus duplex ageing	600	0.5	52.9	83 ± 20	113 ± 17
Solution-treated plus single ageing with faster heating rate	600	0.5	52.3	139 ± 22	187 ± 16

The variation in linear density of grain boundary α-phase, *i.e.* total coverage of grain boundary (in %) for the as-built and the solution-treated samples as a function of different

ageing conditions is shown in Fig. 9. The grain boundary α-phase was analysed over a range of grain boundaries across the sample. For single ageing of the as-built samples with faster heating rate, the linear density of grain boundary α-phase increased with ageing temperature. The samples aged at 500 °C and 600 °C showed discontinuous grain boundary α-phase. However, continuous grain boundary α-phase was observed after ageing at 700 °C. It is important to note here that the solution-treated single-aged sample showed very high grain boundary coverage when compared with the fast-heated single-aged as-built sample aged at the same temperature (600 °C). The slow-heated and duplex aged sample also showed the presence of continuous grain boundary α-phase, as can be seen in Fig. 9.

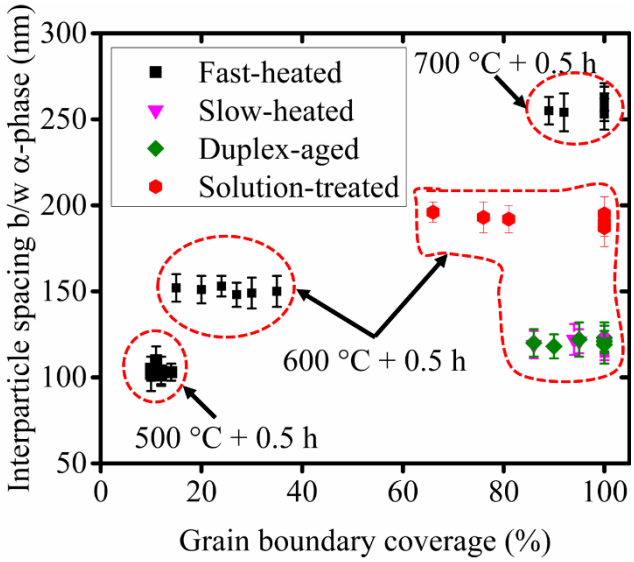

Fig. 9. The characteristic variation in linear density of grain boundary α-phase precipitates along with interparticle spacing between intragranular α-phase precipitates for the as-built and the solution-treated samples as a function of ageing temperature.

3.2. Microhardness and tensile test results

The hardness and the tensile test results are presented in Table 6. The hardness values of the as-built and the solution-treated samples before ageing remained within the error bars and were found to be 311 ± 8 Hv and 305 ± 5 Hv respectively. The removal of sub-structures after solution treatment does not affect the hardness values significantly. Hence, it is stated that the sub-structures do not act as barriers to the dislocations or do not act as the nucleation points

that can possibly affect the subsequent precipitation of α-phase during ageing. The as-built sample showed the hardness value (311 ± 8 Hv) very close to the value obtained for wrought Ti-5553 β-Ti alloy after solution treatment (288 ± 5 Hv) [20]. The small difference in the hardness value is because of the coarser β grain size (245 ± 65 μm) for wrought samples in the literature [20] when compared to the β grain size in as-built samples (184 ± 64 μm). The hardness value remained low for the single-aged (600 °C/0.5 h) solution-treated sample (400 ± 5 Hv) when compared to the fast-heated single-aged (600 °C/0.5 h) as-built sample (424 ± 5 Hv).

For single ageing of the as-built samples with the faster heating rate approach, the highest microhardness values were obtained for samples aged at 500 °C. The hardness value increased with ageing time (0.5 h to 6 h) at 500 °C. The samples aged at 700 °C showed the lowest hardness. The hardness of the samples decreased as the ageing time was increased at 600 °C, however, ageing time did not affect the hardness values after ageing at 700 °C. The slow-heated single-aged and duplex-aged samples showed similar microhardness values. These samples also showed a higher hardness when compared to the fast-heated single-aged samples (as-built and solution-treated).

Tensile test curves of the aged (600 °C + 0.5 h) Ti-5553 β-Ti alloy samples following different ageing approaches are shown in Fig. 10. It can be seen from Table 6 that the slow-heated single-aged and the duplex-aged samples showed similar tensile properties; whilst possess higher ultimate tensile strength when compared to fast-heated single-aged as-built and solution-treated samples. This trend in ultimate tensile strength for slow-heated single-aged and duplex-aged samples is similar to the hardness trend. The slow-heated single-aged and the duplex-aged samples showed lower ductility than fast-heated single-aged as-built and solution-treated single-aged samples. The fast-heated single-aged as-built sample showed a good balance in mechanical properties (Table 6); the ultimate tensile strength for this sample is

higher than the solution-treated single-aged samples. This sample showed the highest ductility amongst all the aged samples. Khodabakhshi *et al.* [21] reported that the ultimate tensile strength of the metals and alloys is approximately three times the microhardness values; this relationship also holds true for the current work (Table 6). It is also important to note here that the obtained microhardness and tensile test results for the current work were found to be comparable (Table 6) with the available microhardness and tensile test results in the literature for SLM-built [14] and wrought [1,22] Ti-5553 β-Ti alloy. This boosts confidence in exploring the DLD process in a production application.

Table 6. Vickers microhardness and tensile test results for additively manufactured Ti-5553 β-Ti alloy as a function of different ageing conditions. The data presented illustrate the microhardness and tensile test results for the samples aged via single ageing with faster heating rate, single ageing with slower heating rate, duplex ageing, and single ageing with faster heating rate after solution treatment. The table also shows a comparison of the microhardness and tensile test results from the current work with the available microhardness and tensile test results in the literature for additively manufactured [14] and wrought [1,22] Ti-5553 β-Ti alloy.

Approach	Heat treatment condition		Hardness ($Hv_{0.5}$)	$\sim\sigma_{UTS}$ (MPa)	$\sim\sigma_{0.2}$ (MPa)	δ (%)
	Temperature (°C)	Time (h)				
As-built plus single ageing with faster heating rate	500	0.5	471 ± 4	-	-	-
		6	488 ± 4	-	-	-
	600	0.5	424 ± 5	1345 ± 5	1060 ± 5	11.6 ± 0.5
		6	410 ± 3	-	-	-
	700	0.5	344 ± 3	-	-	-
		6	345 ± 4	-	-	-
As-built plus single ageing with slower heating rate	600	0.5	462 ± 8	1380 ± 8	1200 ± 6	4.2 ± 0.2
As-built plus duplex ageing	600	0.5	459 ± 8	1365 ± 4	1200 ± 4	4 ± 0.3
Solution-treated plus single ageing with faster heating rate	600	0.5	400 ± 5	1150 ± 3	925 ± 4	8.2 ± 0.4
Wrought material (single ageing with faster heating rate) [1,22]	600	0.5	476	1265 ± 5	1173 ± 4	9 ± 0.7
		1	490	-	-	-
Wrought material (duplex aged) [1]	600	1		1368 ± 11	-	2 ± 0.4
Additively manufactured (single ageing with faster heating rate) [14]	500	1	475 ± 20	-	-	-
	600	1	416 ± 16	1371 ± 21	1332 ± 32	3.5 ± 0.6
	700	1	362 ± 14	-	-	-

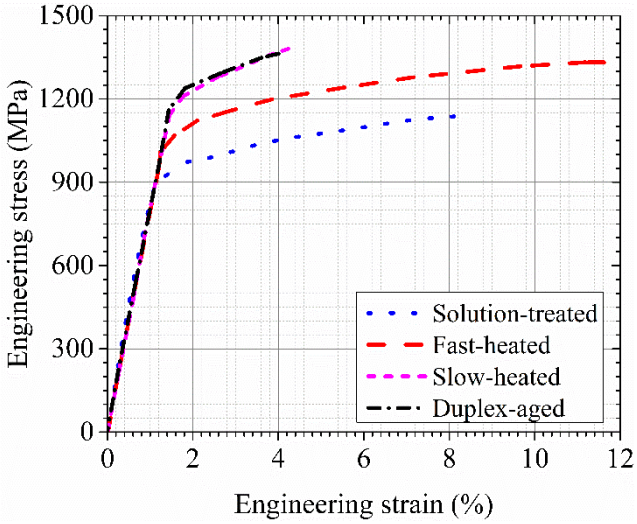

Fig. 10. The tensile test curves for the aged (600 °C + 0.5 h) Ti-5553 β-Ti alloy following different ageing approaches. The tests were conducted at room temperature with a strain rate of 10^{-4}/s.

4. Discussion

4.1. Development of microstructure for as-built samples

The formation of solely β-phase in the microstructure of the as-built sample is attributed to the rapid cooling during deposition. The elongation of β-phase grains along the build height is attributed to the temperature gradient along the build height during deposition. The high-temperature gradient towards the bottom of the sample led to columnar solidification, however, a reduced temperature gradient at the top of the samples resulted in a higher fraction of equiaxed β-phase grains [12,23]. The crystallisation of undercooled melt takes in the most preferred growth directions [12], which is the <100> for BCC structures [24].

The formation of the sub-structures can be understood from the constitutional undercooling [23,25]. The reduction in the temperature gradient ahead of the planar interface increases the undercooling leading to increased outgrowth away from the interface. Hence, the cell structure is formed, which causes the rejection of solute causing the reduction in equilibrium solidification temperature [23]. When the n^{th} melt pool (Fig. 2 (b)) is deposited over the $(n-1)^{th}$ melt pool (already deposited material), then the top of the material will have

443 approximately similar temperature as that of the surrounding which will decrease the
444 temperature gradient at the top of the n^{th} melt pool, *i.e.* below the $(n+1)^{th}$ scan track (Fig. 2 (b)).
445 Hence, we have seen cellular sub-structures just below the $(n+1)^{th}$ scan track (Fig. 2 (b)). The
446 segregation of the solute elements is dependent on their solubility limits in the liquid and the
447 solid states. Depending on the solubility, the solid may either take excess solute from the liquid
448 or reject solute into the liquid. The redistribution of the solute elements can be understood with
449 the help of equilibrium segregation coefficient (k) (Equation (1)) that is defined as the ratio of
450 solute concentration in the solid (C_s) and the liquid (C_L) at the solid interface at any given
451 temperature T.

452 $$k = C_s / C_L \quad (1)$$

453 The solubility of a solute is dependent on the temperature. At a particular temperature
454 when $k < 1$, the solute solubility is greater in the liquid phase relative to the solid. For $k > 1$,
455 the solute solubility is greater in the solid phase. This means that when the solute solubility
456 decreases for a particular phase then it cannot hold the solute further and rejects it to another
457 phase during solidification. From Ti-Mo and Ti-Cr phase diagrams, the k values were
458 calculated to be greater and less than 1, respectively. This implies that Mo will be rejected to
459 the solid phase, *i.e.*, the core of the sub-structures, however, Cr will be rejected to the sub-
460 structure boundaries. For the remaining solute elements, the k values were calculated to be
461 approximately equal to 1, which indicates that they are uniformly distributed across the sub-
462 structures. This correlates to observations from EDS analysis (Table 3).

463 Whilst depositing the n^{th} melt pool, the bottom portion of the melt pool will be in touch
464 with the already deposited material ($(n-1)^{th}$ melt pool). This will lead to a higher temperature
465 gradient in the bottom part of the n^{th} melt pool (region above n^{th} scan track in Fig. 2 (b)). This

higher temperature gradient during solidification will reduce the outgrowth leading to no sub-structures in this region, as can be seen just above n^{th} scan track in Fig. 2 (b).

4.2. Development of microstructure for aged samples

Previously published literature [26] has shown higher dislocation density in the as-built samples. This is due to the rapid solidification of the sample during deposition. However, the heat treatment of the sample will cause the annihilation of the dislocations [27]. Hence, the solution-treated sample will have a lower number density of dislocations. These dislocations in the sample will act as the nucleation sites for the α-phase precipitation. Hence, the refinement of intragranular α-phase for the as-built sample in comparison to the solution-treated sample is attributed to the higher number density of dislocations in the as-built condition. The EDS analysis (Table 4) of the aged samples have also shown that the sub-structure core are rich in Mo, but depleted in Cr, whilst sub-structure boundaries are rich in Cr and depleted in Mo. This is same as the EDS analysis (Table 3) for the as-built samples. The value of Mo equivalent for the sub-structure free region, the core of the sub-structure and the sub-structure boundary was calculated as ~8.3. The representation of Mo equivalent is presented in Equation 2. This was taken from reference [28]. The Mo equivalent is almost the same for all the regions. Mo equivalent controls the precipitation temperature for the phases. Having the same Mo equivalent will lead to same precipitation temperature for α-phase in all these different regions. Hence, this is the reason for getting the uniform microstructure throughout although we have seen Mo and Cr segregation across the sub-structures, but both are β-phase stabilisers.

$$[Mo]_{eq} = [Mo] + 0.22[Ta] + 0.28[Nb] + 0.44[W] + 0.67[V] + 1.6[Cr] + 1.25[Ni] + 1.7[Co] + 2.9[Fe] - 1.0[Al] \quad (2)$$

The formation of extremely refined microstructure for the slow-heated single-aged and the duplex-aged samples is because of ω-phase-assisted α-phase nucleation. The refinement of the intragranular α-phase for the fast-heated single-aged samples after ageing at a lower

491 temperature (500 °C and 600 °C), and the slow-heated single-aged and the duplex-aged
492 samples may also result in a loss of ductility, as reported in [29]. However, the ductility is
493 reported [6] to be dominated by the grain boundary α-phase. The authors reported an empirical
494 relation between ductility and grain boundary α-phase based on their experimental validation.
495 They reported that a higher degree of discontinuity in the grain boundary α-phase is directly
496 proportional to an increase in ductility. For the current work, discontinuous grain boundary α-
497 phase was observed after single ageing the as-built samples with the faster heating rate at 500
498 °C and 600 °C. Discontinuous grain boundary and refined intragranular α-phase for as-built
499 samples after ageing are desired for simultaneously achieving high ductility and strength.

500 As understood from the grain boundary α-phase data (Fig. 9) for fast-heated single-aged
501 as-built samples, it is stated the grain boundary α primarily starts forming with the
502 heterogeneous nucleation at the grain boundaries and then grows due to diffusion of Al and O
503 (α stabilizing elements) from the surroundings to the grain boundary α [6]. The diffusion of Al
504 and O from the grain boundary surroundings makes the region rich in β-stabilisers, hence,
505 leading to the formation of PFZ. The growth of the α-phase at grain boundary allows the
506 different nucleants at grain boundary to connect and form a continuous grain boundary α. The
507 nucleation and growth of the α-phase is a temperature-dependent process; hence, a larger rate
508 of diffusion happens at 700 °C leading to continuous grain boundary α-phase.

509 4.3. Effect of microstructure on microhardness and tensile properties

510 The effect of interparticle spacing on the mechanical properties in Ti–6Mo–5V–3Al–2Fe
511 β-Ti alloy has been considered previously [19]. This work suggests that the variation in
512 interparticle spacing observed in the present work would contribute to a change in mechanical
513 properties. The reduction in the interparticle spacing is directly linked to the increase in strength
514 and hardness [10,16,30]. Therefore, it is concluded that the increase in hardness of ~24 Hv for

515 the as-built sample in comparison to solution-treated sample after ageing with faster heating
516 rate is solely due to the reduction in the interparticle spacing between the α-phase. A similar
517 proportional change is expected in the ultimate tensile strength of the material [31,32] as seen
518 from the tensile test results (Table 6).

519 The observation of the highest microhardness and ultimate tensile strength for the slow-
520 heated single-aged and the duplex-aged samples is because of the extremely refined
521 microstructure. This makes the dislocations to pile up into more interfaces due to reduced
522 interparticle spacing, and the movement is restricted; whilst relatively coarser microstructure,
523 as observed for fast-heated single-aged as-built and solution-treated samples, allows the greater
524 movement of dislocations between interparticle spacing; leading to a decrease in hardness and
525 ultimate tensile strength values. However, the fast-heated single-aged as-built sample showed
526 higher microhardness and ultimate tensile strength values than the fast-heated single-aged
527 solution treated sample due to relatively finer microstructure.

528 The hardness values decreased with temperature due to an increase in interparticle spacing
529 in the microstructure. The samples aged at 500 °C showed the highest hardness amongst the
530 single aged sample using single ageing with faster heating rate. This is attributed to the reduced
531 interparticle spacing. The further increment in hardness with ageing time at this temperature
532 was because of the increased number density of α-phase (as stated above) leading to a further
533 reduction in interparticle spacing (Table 5). At 700 °C, the coarsened α-phase and the reduced
534 volume fraction led to the increase in interparticle spacing; hence, leading to a decrease in
535 hardness. The ageing time at 700 °C did not cause any change in the hardness because the
536 interparticle spacing and volume fraction of α-phase remained constant with ageing time. The
537 drop in the hardness with ageing time at 600 °C is because of the coarsening of the α-phase
538 leading to increased interparticle spacing.

A correlation between the microhardness values and the interparticle spacing between the α-phase (d) was established for all the aged samples. A high value of correlation coefficient, $R^2 = 0.99$, was observed for the fitted regression lines. The mean interparticle spacing between the α-phase was considered as the best microstructural feature to control the microhardness values. The dependence of microhardness and the interparticle spacing between the α-phase is represented in Fig. 11 (a), and the relation is given in Equation 3. A similar correlation was obtained between the yield stress ($\sigma_{0.2}$) values and the interparticle spacing, as shown in Fig. 11 (b). A high value of correlation coefficient, $R^2 = 0.97$, was observed for the fitted regression lines. The relation is given in Equation 4.

$$H_v = 340 + 158/\sqrt{d} \quad (3)$$

$$\sigma_{0.2} = 870 + 15086/\sqrt{d} \quad (4)$$

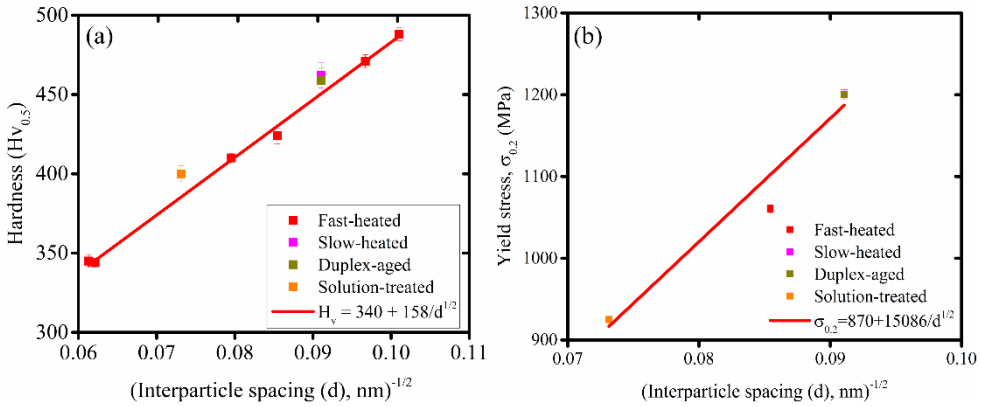

Fig. 11. The variation of mean (a) hardness and (b) yield stress with the inverse of the square root of mean interparticle spacing between the α-phase after ageing the AM Ti-5553 β-Ti alloy samples.

The slow-heated single-aged and the duplex-aged samples showed lower ductility than the fast-heated single-aged as-built and solution-treated samples. The extreme refinement of the α-phase leads to a flatter interface between the intragranular precipitate and the grain boundary. Therefore, higher stress is required to deform the samples which leads to the formation of voids and expansion mainly along the interface; subsequently leading to intergranular fracture [1]. Also, the presence of continuous grain boundary α-phase plays an important role in the

reduction of the ductility for the slow-heated single-aged and the duplex-aged samples [6]. The solution-treated single-aged sample showed the least ultimate tensile strength amongst all the aged samples, but higher ductility than the slow-heated single-aged and the duplex-aged samples. The least ultimate strength was because of the coarsest microstructure leading to larger interparticle spacing (Table 5); however, the non-uniform size and distribution of intragranular α-phase precipitates results in distinct lamella spacing and undulating interface that assimilates more plastic dissipation leading to higher ductility [1]. The fast-heated single-aged as-built sample showed a good balance in mechanical properties (Table 6). This sample showed the highest ductility amongst all the aged samples. This is because of the presence of discontinuous grain boundary α-phase that can be linked with the much ductile nature of the sample as stated above [6]. In literature [6], a very complex heat treatment method was used for laser melting deposited Ti alloy samples to obtain the discontinuous grain boundary α-phase to improve the ductility (~12.3%) of the material; however, the current work shows very simple steps to obtain the higher ductility (~11.6%). It is also important to note here that the tensile properties (Table 6) obtained from the current work are comparable with the wrought and the SLM-built alloys. This boosts confidence in exploring the DLD process in a production application.

When Fig. 9 and Table 6 are correlated then it can be understood that the strength of Ti-5553 β-Ti alloy can be improved by reducing the interparticle spacing between the α-phase precipitates. However, the ductility of the material can be improved by either getting the coarser intragranular α-phase or getting the discontinuous grain boundary α-phase. Obtaining refined intragranular α-phase and discontinuous grain boundary α-phase in a single microstructure will lead to balanced mechanical properties for the material. This is what has happened with the fast-heated single-aged as-built sample aged at 600 °C for 0.5 h.

Conclusions

The following conclusions can be drawn from this work:

1. A unique microstructure with refined intragranular and discontinuous grain boundary α-phase can be obtained by directly ageing (using fast heating rate) the as-built samples at ageing temperature (600 °C + 0.5 h). This microstructure produced a good balance in mechanical properties (UTS = 1345 ± 5 MPa and δ = 11.6 ± 0.5 %).
2. The as-built samples showed relatively refined intragranular α-phase after single ageing with a faster heating rate when compared to solution-treated plus aged samples. This led to higher hardness and ultimate tensile strength values.
3. The duplex-aged and slow-heated single-aged samples showed similar microstructure and mechanical properties. These samples showed maximum hardness and ultimate tensile strength values, but lowest ductility; due to extreme refinement of the intragranular α-phase.
4. The interparticle spacing between the α-phase (d) showed a correlation with microhardness ($H_v = 340 + 158/\sqrt{d}$) and yield stress ($\sigma_{0.2} = 870 + 15086/\sqrt{d}$) values for all the aged samples.
5. The obtained microhardness and tensile test results for the current work were found to be comparable with the available microhardness and tensile test results in the literature for SLM-built and wrought Ti-5553 β-Ti alloy. This boosts confidence in exploring the DLD process in a production application.

Acknowledgement

MEF is grateful for funding from the Lloyd's Register Foundation (LRF), a charitable foundation helping to protect life and property by supporting engineering-related education, public engagement and the application of research.

References

[1] L. Ren, W. Xiao, W. Han, C. Ma, L. Zhou, Influence of duplex ageing on secondary α precipitates and mechanical properties of the near β -Ti alloy Ti-55531, Mater. Charact. 144 (2018) 1–8. doi:10.1016/j.matchar.2018.06.025.

[2] J. Chen, W. Xiao, M.S. Dargusch, C. Ma, The dependence of isothermal ω precipitation on the quenching rate in a metastable β-Ti alloy, Sci. Rep. 5 (2015) 14632. doi:10.1038/srep14632.

[3] A. Settefrati, M. Dehmas, G. Geandier, B. Denand, E. Aeby-Gautier, B. Appolaire, G. Khelifati, J. Delfosse, Precipitation sequences in beta metastable phase of Ti-5553 alloy during ageing, Proc. 12th World Conf. Titan. (2011) 468–472.

[4] S. Shekhar, R. Sarkar, S.K. Kar, A. Bhattacharjee, Effect of solution treatment and aging on microstructure and tensile properties of high strength β titanium alloy, Ti–5Al–5V–5Mo–3Cr, Mater. Des. 66 (2015) 596–610. doi:10.1016/j.matdes.2014.04.015.

[5] P. Manda, V. Singh, U. Chakkingal, A.K. Singh, Development of α precipitates in metastable Ti-5Al-5Mo-5V-3Cr and similar alloys, Mater. Charact. 120 (2016) 220–228. doi:10.1016/j.matchar.2016.09.005.

[6] C.M. Liu, H.M. Wang, X.J. Tian, D. Liu, Development of a pre-heat treatment for obtaining discontinuous grain boundary α in laser melting deposited Ti-5Al-5Mo-5V-1Cr-1Fe alloy, Mater. Sci. Eng. A. 604 (2014) 176–182. doi:10.1016/j.msea.2014.03.028.

[7] Y. Zheng, R.E.A. Williams, D. Wang, R. Shi, S. Nag, P. Kami, J.M. Sosa, R. Banerjee, Y. Wang, H.L. Fraser, Role of ω phase in the formation of extremely refined intragranular α precipitates in metastable β-titanium alloys, Acta Mater. 103 (2016) 850–858. doi:10.1016/j.actamat.2015.11.020.

[8] S. Nag, A. Devaraj, R. Srinivasan, R.E.A. Williams, N. Gupta, G.B. Viswanathan, J.S. Tiley, S. Banerjee, S.G. Srinivasan, H.L. Fraser, R. Banerjee, Novel mixed-mode phase transition involving a composition-dependent displacive component, Phys. Rev. Lett. 106 (2011) 7–10. doi:10.1103/PhysRevLett.106.245701.

[9] D. Sharma, D. Parfitt, B. Chen, B. Roebuck, D.A. Venero, S.R. Kada, D. Fabijanic, M.E. Fitzpatrick, Influence of cooling rate on the precipitation kinetics of nanoscale isothermal ω-phase in metastable β-Ti alloy, Ti–5Al–5Mo–5V–3Cr, J. Alloys Compd. 859 (2021) 157822. doi:10.1016/j.jallcom.2020.157822.

[10] M. Qian, W. Xu, M. Brandt, H.P. Tang, Additive manufacturing and postprocessing of Ti-6Al-4V for superior mechanical properties, MRS Bull. 41 (2016) 775–783. doi:10.1557/mrs.2016.215.

[11] N. Shamsaei, A. Yadollahi, L. Bian, S.M. Thompson, An overview of direct laser deposition for additive manufacturing; Part II: Mechanical behavior, process parameter optimization and control, Addit. Manuf. 8 (2015) 12–35. doi:10.1016/j.addma.2015.07.002.

[12] H. Schwab, F. Palm, U. Kühn, J. Eckert, Microstructure and mechanical properties of the near-beta titanium alloy Ti-5553 processed by selective laser melting, Mater. Des. 105 (2016) 75–80. doi:10.1016/j.matdes.2016.04.103.

[13] H. Schwab, M. Bönisch, L. Giebeler, T. Gustmann, J. Eckert, U. Kühn, Processing of

653 Ti-5553 with improved mechanical properties via an in-situ heat treatment combining
654 selective laser melting and substrate plate heating, Mater. Des. 130 (2017) 83–89.
655 doi:10.1016/j.matdes.2017.05.010.

656 [14] H.D. Carlton, K.D. Klein, J.W. Elmer, Evolution of microstructure and mechanical
657 properties of selective laser melted Ti-5Al-5V-5Mo-3Cr after heat treatments,
658 Sci. Technol. Weld. Join. 24 (2019) 465–473. doi:10.1080/13621718.2019.1594589.

659 [15] C. Liu, Y. Lu, X. Tian, D. Liu, Influence of continuous grain boundary α on ductility of
660 laser melting deposited titanium alloys, Mater. Sci. Eng. A. 661 (2016) 145–151.
661 doi:10.1016/j.msea.2016.03.034.

662 [16] H. Sharma, D. Parfitt, A.K. Syed, D. Wimpenny, E. Muzangaza, G. Baxter, B. Chen, A
663 critical evaluation of the microstructural gradient along the build direction in electron
664 beam melted Ti-6Al-4V alloy, Mater. Sci. Eng. A. 744 (2019) 182–194.
665 doi:10.1016/j.msea.2018.12.016.

666 [17] J. Coakley, V.A. Vorontsov, N.G. Jones, A. Radecka, P.A.J. Bagot, K.C. Littrell, R.K.
667 Heenan, F. Hu, A.P. Magyar, D.C. Bell, D. Dye, Precipitation processes in the beta-
668 titanium alloy Ti-5Al-5Mo-5V-3Cr, J. Alloys Compd. 646 (2015) 946–953.
669 doi:10.1016/j.jallcom.2015.05.251.

670 [18] J. Coakley, V.A. Vorontsov, K.C. Littrell, R.K. Heenan, M. Ohnuma, N.G. Jones, D.
671 Dye, Nanoprecipitation in a beta-titanium alloy, J. Alloys Compd. 623 (2015) 146–156.
672 doi:10.1016/j.jallcom.2014.10.038.

673 [19] H. Zhang, C. Wang, S. Zhang, G. Zhou, L. Chen, Evolution of secondary α phase during
674 aging treatment in novel near Ti-6Mo-5V-3Al-2Fe Alloy, Mater. 11 (2018) 2283.
675 doi:10.3390/ma11112283.

676 [20] B.Z. Jiang, S. Emura, K. Tsuchiya, Microstructures and mechanical properties of Ti-
677 5553 alloy processed by high-pressure torsion, IOP Conf. Ser. Mater. Sci. Eng. 63
678 (2014) 012069. doi:10.1088/1757-899X/63/1/012069.

679 [21] F. Khodabakhshi, M. Haghshenas, H. Eskandari, B. Koohbor, Hardness-strength
680 relationships in fine and ultra-fine grained metals processed through constrained groove
681 pressing, Mater. Sci. Eng. A. 636 (2015) 331–339. doi:10.1016/j.msea.2015.03.122.

682 [22] S.H. Xu, Y. Liu, B. Liu, X. Wang, Z.X. Chen, Microstructural evolution and mechanical
683 properties of Ti–5Al–5Mo–5V–3Cr alloy by heat treatment with continuous temperature
684 gradient, Trans. Nonferrous Met. Soc. China. 28 (2018) 273–281. doi:10.1016/S1003-
685 6326(18)64660-6.

686 [23] D.A. Porter, K.E. Easterling, Phase Transformations in Metals and Alloys, Second ed.,
687 Springer-Science + Business Media, Hong Kong, 1992.

688 [24] B. Vrancken, L. Thijs, J. Kruth, J. Van Humbeeck, Microstructure and mechanical
689 properties of a novel β titanium metallic composite by selective laser melting, Acta
690 Mater. 68 (2014) 150–158. doi:10.1016/j.actamat.2014.01.018.

691 [25] K. Saeidi, X. Gao, Y. Zhong, Z.J. Shen, Hardened austenite steel with columnar sub-
692 grain structure formed by laser melting, Mater. Sci. Eng. A. 625 (2015) 221–229.
693 doi:10.1016/j.msea.2014.12.018.

694 [26] R. Acevedo, P. Sedlak, R. Kolman, M. Fredel, Residual stress analysis of additive
695 manufacturing of metallic parts using ultrasonic waves: State of the art review, J. Mater.

696 Res. Technol. (2020) 1–21. doi:10.1016/j.jmrt.2020.05.092.

697 [27] M. Hu, W.D. Fei, C.K. Yao, Effect of heat treatment on dislocation states and work
698 hardening behaviors of SiCw/6061Al composite, Mater. Lett. 56 (2002) 637–641.
699 doi:10.1016/S0167-577X(02)00568-2.

700 [28] P. Manda, U. Chakkingal, A.K. Singh, Hardness characteristic and shear band formation
701 in metastable β-titanium alloys, Mater. Charact. 96 (2014) 151–157.
702 doi:10.1016/j.matchar.2014.07.027.

703 [29] Z.D. Lü, C.J. Zhang, Z.X. Du, J.C. Han, S.Z. Zhang, F. Yang, Y.Y. Chen, Relationship
704 between microstructure and tensile properties on a near-β titanium alloy after
705 multidirectional forging and heat treatment, Rare Met. 38 (2019) 336–342.
706 doi:10.1007/s12598-018-1159-y.

707 [30] S.A. Mantri, D. Choudhuri, T. Alam, G.B. Viswanathan, J.M. Sosa, H.L. Fraser, R.
708 Banerjee, Tuning the scale of α precipitates in β-titanium alloys for achieving high
709 strength, Scr. Mater. 154 (2018) 139–144. doi:10.1016/j.scriptamat.2018.05.040.

710 [31] A. Casagrande, G.P. Cammarota, L. Micele, Relationship between fatigue limit and
711 Vickers hardness in steels, Mater. Sci. Eng. A. 528 (2011) 3468–3473.
712 doi:10.1016/j.msea.2011.01.040.

713 [32] I. Brooks, P. Lin, G. Palumbo, G.D. Hibbard, U. Erb, Analysis of hardness – tensile
714 strength relationships for electroformed nanocrystalline materials, Mater. Sci. Eng. A.
715 491 (2008) 412–419. doi:10.1016/j.msea.2008.02.015.

716